



























TOI-3235 b: a transiting giant planet around an M4 dwarf star

MELISSA J. HOBSON ^{1,2} ANDRÉS JORDÁN ^{3,2,4} E. M. BRYANT ^{5,6,7} R. BRAHM ^{3,2,4} D. BAYLISS ⁵
J. D. HARTMAN ⁸ G. Á. BAKOS ⁸ TH. HENNING¹ JOSE MANUEL ALMENARA ⁹ KHALID BARKAOUI ^{10,11,12}
ZOUHAIR BENKHALDOUN ¹³ XAVIER BONFILS ⁹ FRANÇOIS BOUCHY¹⁴ DAVID CHARBONNEAU¹⁵ MARION COINTEPAS^{9,14}
KAREN A. COLLINS ¹⁵ JASON D. EASTMAN ¹⁵ MOURAD GHACHOUI^{10,13} MICHAËL GILLON ¹⁰ ROBERT F. GOEKE¹⁶
KEITH HORNE ¹⁷ JONATHAN M. IRWIN¹⁸ EMMANUEL JEHIN ¹⁹ JON M. JENKINS ²⁰ DAVID W. LATHAM ¹⁵
DAN MOLDOVAN²¹ FELIPE MURGAS ^{9,22,23} FRANCISCO J. POZUELOS ^{10,19,24} GEORGE R. RICKER ¹⁶
RICHARD P. SCHWARZ ¹⁵ S. SEAGER ^{16,25,26} GREGOR SRDOC²⁷ STEPHANIE STRIEGEL²⁸ MATHILDE TIMMERMANS¹⁰
ANDREW VANDERBURG ¹⁶ ROLAND VANDERSPEK ¹⁶ AND JOSHUA N. WINN ²⁹

¹Max Planck Institute for Astronomy, Königstuhl 17, 69117 - Heidelberg, Germany

²Millennium Institute of Astrophysics (MAS), Nuncio Monseñor Sótero Sanz 100, Providencia, Santiago, Chile

³Facultad de Ingeniería y Ciencias, Universidad Adolfo Ibáñez, Av. Diagonal las Torres 2640, Peñalolén, Santiago, Chile

⁴Data Observatory Foundation, Santiago, Chile

⁵Department of Physics, University of Warwick, Gibbet Hill Road, Coventry CV4 7AL, UK

⁶Centre for Exoplanets and Habitability, University of Warwick, Gibbet Hill Road, Coventry CV4 7AL, UK

⁷Mullard Space Science Laboratory, University College London, Holmbury St Mary, Dorking, Surrey, RH5 6NT, UK

⁸Department of Astrophysical Sciences, Princeton University, NJ 08544, USA

⁹Univ. Grenoble Alpes, CNRS, IPAG, F-38000 Grenoble, France

¹⁰Astrobiology Research Unit, Université de Liège, 19C Allée du 6 Août, 4000 Liège, Belgium

¹¹Department of Earth, Atmospheric and Planetary Science, Massachusetts Institute of Technology, 77 Massachusetts Avenue, Cambridge, MA 02139, USA

¹²Instituto de Astrofísica de Canarias (IAC), Calle Vía Láctea s/n, 38200, La Laguna, Tenerife, Spain

¹³Oukaimeden Observatory, High Energy Physics and Astrophysics Laboratory, Faculty of sciences Semlalia, Cadi Ayyad University, Marrakech, Morocco

¹⁴Observatoire de Genève, Département d'Astronomie, Université de Genève, Chemin Pegasi 51b, 1290 Versoix, Switzerland

¹⁵Center for Astrophysics | Harvard & Smithsonian, 60 Garden St., Cambridge, MA 02138, USA

¹⁶Department of Physics and Kavli Institute for Astrophysics and Space Research, Massachusetts Institute of Technology, Cambridge, MA 02139, USA

¹⁷SUPA Physics and Astronomy, University of St. Andrews, Fife, KY16 9SS Scotland, UK

¹⁸Institute of Astronomy, University of Cambridge, Madingley Road, Cambridge, CB3 0HA, United Kingdom

¹⁹Space sciences, Technologies and Astrophysics Research (STAR) Institute, Université de Liège, Belgium

²⁰NASA Ames Research Center, Moffett Field, CA 94035, USA

²¹Google, Cambridge, MA, USA

²²Instituto de Astrofísica de Canarias (IAC), E-38200 La Laguna, Tenerife, Spain

²³Dept. Astrofísica, Universidad de La Laguna (ULL), E-38206 La Laguna, Tenerife, Spain

²⁴Instituto de Astrofísica de Andalucía (IAA-CSIC), Glorieta de la Astronomía s/n, 18008 Granada, Spain

²⁵Department of Earth, Atmospheric and Planetary Sciences, Massachusetts Institute of Technology, Cambridge, MA 02139, USA

²⁶Department of Aeronautics and Astronautics, MIT, 77 Massachusetts Avenue, Cambridge, MA 02139, USA

²⁷Kotizarovci Observatory, Sarsoni 90, 51216 Viskovo, Croatia

²⁸San Jose State University, 1 Washington Sq, San Jose, CA 95192, USA

²⁹Department of Astrophysical Sciences, Princeton University, 4 Ivy Lane, Princeton, NJ 08544, USA

ABSTRACT

We present the discovery of TOI-3235 b, a short-period Jupiter orbiting an M-dwarf with a stellar mass close to the critical mass at which stars transition from partially to fully convective. TOI-3235 b was first identified as a candidate from *TESS* photometry, and confirmed with radial velocities from ESPRESSO, and ground-based photometry from HATSouth, MEarth-South, TRAPPIST-

South, LCOGT, and ExTrA. We find that the planet has a mass of $0.665 \pm 0.025 M_J$ and a radius of $1.017 \pm 0.044 R_J$. It orbits close to its host star, with an orbital period of 2.5926 d, but has an equilibrium temperature of ≈ 604 K, well below the expected threshold for radius inflation of hot Jupiters. The host star has a mass of $0.3939 \pm 0.0030 M_\odot$, a radius of $0.3697 \pm 0.0018 R_\odot$, an effective temperature of 3389 K, and a J-band magnitude of 11.706 ± 0.025 . Current planet formation models do not predict the existence of gas giants such as TOI-3235 b around such low-mass stars. With a high transmission spectroscopy metric, TOI-3235 b is one of the best-suited giants orbiting M-dwarfs for atmospheric characterization.

Keywords: planetary systems — stars: individual (TOI-3235) — techniques: spectroscopic, photometric

1. INTRODUCTION

While planets around M-dwarf stars are extremely abundant (e.g. Dressing & Charbonneau 2015; Hirano et al. 2018; Mulders 2018; Hsu et al. 2020), the vast majority of these planets are smaller than Neptune, particularly around less massive M-dwarfs ($M < 0.5 M_\odot$). Standard core-accretion formation models have long predicted few Jovian-mass planets around these less massive M-dwarfs (e.g. Laughlin et al. 2004, who also anticipate a particular scarcity of short-period giant planets). More recent implementations such as the Bern model (Burn et al. 2021) reproduce the low-mass planet population very well, but predict few gas giants around all M-dwarfs, and cannot produce them around later M-dwarfs with $M < 0.5 M_\odot$ without fine-tuning of the planetary migration (Schlecker et al. 2022). Even prior to the *Transiting Exoplanet Survey Satellite* mission (*TESS*, Ricker et al. 2015), there were discoveries that challenged this (such as Kepler-45 b, Johnson et al. 2012; HATS-6 b, Hartman et al. 2015; NGTS-1 b, Bayliss et al. 2018). More recently, both *TESS* and radial velocity (RV) surveys have added to the known giant planets orbiting low-mass stars (e.g. GJ 3512 b, Morales et al. 2019; TOI-3884 b, Almenara et al. 2022), suggesting a potential alternative formation pathway such as gravitational instability (e.g. Boss 2006). However, as noted by Schlecker et al. (2022), gravitational instability is expected to form very massive planets of $\approx 10 M_J$ on large orbits, while the planets found to date are mainly of Jupiter mass and many have short orbital periods. Likewise, most of these planets orbit early M-dwarfs, for which the Bern model can, though rarely, produce gas giants; the first, and until now only, exception was TOI-5205 b (Kanodia et al. 2022), which orbits an M4 star. It is also worth noting that the Bern models normally assume a smooth initial gas surface density distribution in the protoplanetary disk; a non-smooth density distribution could modify the migration history and potentially facilitate the formation of these planets.

In this context, the discovery and characterization of giant planets around M-dwarfs, particularly later M-dwarfs, is of paramount importance to planetary formation and migration theory. Transiting planets confirmed by radial velocities, for which both the mass and radius can be measured, are especially valuable. In this letter, we present the transiting gas giant TOI-3235 b, orbiting an M4 star with a period of 2.5926 days. It is only the second gas giant found to orbit a later M-dwarf on the boundary between partially and fully convective M-dwarfs (Chabrier & Baraffe 1997), and is one of a mere dozen giant planets orbiting M-dwarf stars. The planet was first identified as a candidate by the *TESS* mission, and confirmed with ground-based photometry from HATSouth, MEarth-South, TRAPPIST-South, LCOGT, and ExTrA, and RVs from ESPRESSO.

We present the data in Sect. 2. The analysis is described in Sect. 3. Finally, we discuss and summarize our findings in Sect. 4.

2. OBSERVATIONS

2.1. Photometry

2.1.1. *TESS*

TOI-3235 was observed by the *TESS* primary and extended missions, in sectors 11 (23rd April to 20th May 2019) and 38 (29th April to 26th May 2021) respectively. In both cases, it was observed with camera 2 and CCD 4. The long-cadence data (30-minute cadence for sector 11, 10-minute cadence for sector 38) were initially processed by the Quick-Look Pipeline (QLP, Huang et al. 2020a,b), which uses full-frame images (FFI) calibrated by the *tica* package (Fausnaugh et al. 2020). The QLP detected a planet and it was promoted to a TOI following Guerrero et al. (2021), as noted in the ExoFOP archive ¹. For our analysis, we downloaded the

¹ Located at <https://exofop.ipac.caltech.edu/tess/target.php?id=243641947>

TESS PDCSAP light curves (Stumpe et al. 2012; Smith et al. 2012; Stumpe et al. 2014) processed by the *TESS* Science Processing Operation Center pipeline (SPOC, Jenkins et al. 2016) at NASA Ames Research Center, from the *TESS*-SPOC High Level Science Product on MAST (Caldwell et al. 2020). The SPOC difference image centroiding analysis locates the source of the transit signal to within $3.3 \pm 2.5''$ of the target star (Twicken et al. 2018). The *TESS* light curves are shown in Figure 1, and the data listed in Table 1.

2.1.2. *HATSouth*

HATSouth (Bakos et al. 2013) is a network of 24 telescopes, distributed in three sites at Las Campanas Observatory (LCO) in Chile, the site of the H.E.S.S. gamma-ray observatory in Namibia, and Siding Spring Observatory (SSO) in Australia. Each telescope has a 0.18 m aperture and $4K \times 4K$ front-illuminated CCD cameras. *HATSouth* observed TOI-3235 from 11th February 2017 through 15th May 2017, from all three sites. The data were reduced as described in Penev et al. (2013). The transit was clearly detected, but was not flagged by the automated search due to the high transit depth and the pre-Gaia poor constraint on the stellar size from J-K magnitudes. The light curve is shown in Figure 2 (left panel), and the data are listed in Table 1.

2.1.3. *MEarth-South*

MEarth-South is an array of eight 0.4 m telescopes at the Cerro Tololo Inter-American Observatory (CTIO) in Chile (Nutzman & Charbonneau 2008; Irwin et al. 2015). *M-Earth* observed TOI-3235 with six telescopes on 21st June 2021 in the RG715 filter with 60 s exposure time, obtaining a full transit of TOI-3235.01. The light curves are shown in Figure 2 (right panel), where the data from all six telescopes have been plotted together, and the data are listed in Table 1.

2.1.4. *TRAPPIST-South*

TRAPPIST-South (Jehin et al. 2011; Gillon et al. 2011) is a 0.6 m Ritchey-Chretien robotic telescope at La Silla Observatory in Chile, equipped with a $2K \times 2K$ back-illuminated CCD camera with a pixel scale of $0.65''/\text{pixel}$, resulting a field of view of $22' \times 22'$. A full transit of TOI-3235.01 was observed by *TRAPPIST-South* on 10th May 2022 in the Sloan- z' filter with an exposure time of 100s. We used the *TESS Transit Finder* tool, which is a customised version of the *Tapir* software package (Jensen 2013a), to schedule the observations. Data reduction and photometric measurement

were performed using the *PROSE*² pipeline (Garcia et al. 2021). The light curve is shown in Figure 2 (right panel), and the data are listed in Table 1.

2.1.5. *LCOGT*

The Las Cumbres Observatory global telescope network (*LCOGT*, Brown et al. 2013) is a globally distributed network of 1 m telescopes. The telescopes are equipped with 4096×4096 *SINISTRO* cameras having an image scale of $0''.389$ per pixel, resulting in a $26' \times 26'$ field of view. TOI-3235 was observed by *LCOGT* with the *SINISTRO* instrument at the South Africa Astronomical Observatory (SAAO) site in the Sloan- i' band on 10th June 2021, and at the Cerro Tololo Inter-American Observatory (CTIO) site in the Sloan- g' band on 1st July 2022, full transits of TOI-3235.01 being obtained in both observations. We used the *TESS Transit Finder*, which is a customized version of the *Tapir* software package (Jensen 2013b), to schedule our transit observations. The images were calibrated by the standard *LCOGT BANZAI* pipeline (McCully et al. 2018). The differential photometric data were extracted using *AstroImageJ* (Collins et al. 2017). The light curves are shown in Figure 2 (right panel), and the data listed in Table 1.

2.1.6. *ExTrA*

The *ExTrA* facility (Exoplanets in Transits and their Atmospheres, Bonfils et al. 2015) is composed of a near-infrared (0.85 to $1.55 \mu\text{m}$) multi-object spectrograph fed by three 0.6 m telescopes located at La Silla observatory in Chile. We observed 5 full transits of TOI-3235.01 on 2nd March 2022 (with three telescopes) and on 28th March 2022, 2nd April 2022, 23rd April 2022, and 24th May 2022 (with two telescopes). We observed using the fibers with $8''$ apertures, used the low resolution mode of the spectrograph ($R \sim 20$) and 60-second exposures for all nights. At the focal plane of each telescope, five fiber positioners are used to pick the light from the target and four comparison stars. As comparison stars, we observed 2MASS J13493913-4615443, 2MASS J13515346-4623273, 2MASS J13510825-4612537 and 2MASS J13481046-4615434, with J-magnitude (Skrutskie et al. 2006) and T_{eff} (Gaia Collaboration et al. 2018) similar to TOI-3235. The resulting *ExTrA* data were analyzed using custom data reduction software. The light curves are shown in Figure 2 (right panel), and the data listed in Table 1.

2.2. *Radial Velocities*

² *PROSE*: <https://github.com/lgrcia/prose>

2.2.1. ESPRESSO

ESPRESSO (Echelle SPectrograph for Rocky Exoplanets and Stable Spectroscopic Observations, [Pepe et al. 2021](#)) is an ultra-stable fibre-fed échelle high-resolution spectrograph installed at the incoherent combined Coudé facility of the Very Large Telescope (VLT) in Paranal Observatory, Chile. We observed TOI-3235 with ESPRESSO in HR mode (1 UT, $R \sim 140,000$) between 2nd and 14th February 2022, obtaining 7 spectra under programme ID 108.22B4.001 aka 0108.C-0123(A). The spectra were reduced with the official ESPRESSO DRS v2.3.5 pipeline ([Sosnowska et al. 2015](#); [Modigliani et al. 2020](#)), in the EsoReflex environment ([Freudling et al. 2013](#)). The RVs and bisector spans are listed in Table 2, and the phase-folded RVs and bisector spans are shown in Figure 3 (left panel). Two of the bisector spans are extreme outliers with values of $< -3000 \text{ m s}^{-1}$, and were excluded from the analysis.

3. ANALYSIS

We carried out a joint analysis of the photometric, astrometric and RV data for TOI-3235 b following the methods of [Hartman et al. \(2019\)](#) and [Bakos et al. \(2020\)](#). We fit the light curve data shown in Figures 1 and 2, together with the broad-band catalog photometry and *Gaia* parallax measurement listed in Table 3, and the RV data shown in Figure 3. The model also makes use of the predicted absolute magnitudes in each bandpass from the MIST isochrones and of the extinction, constrained from the SED. We use a [Mandel & Agol \(2002\)](#) transit model with quadratic limb darkening to fit the light curves and assume a Keplerian orbit for fitting the RV measurements. The limb darkening coefficients are allowed to vary, with priors based on the [Claret et al. \(2012, 2013\)](#); [Claret \(2018\)](#) theoretical models. The stellar parameters are constrained using isochrones from version 1.2 of the MIST theoretical stellar evolution models ([Paxton et al. 2011, 2013, 2015](#); [Choi et al. 2016](#); [Dotter 2016](#)). We allow the line of sight extinction A_V to vary in the fit, imposing a maximum of 0.527 mag and a Gaussian prior of 0.055 ± 0.2 mag based on the MWDUST 3D Galactic extinction model ([Bovy et al. 2016](#)).

We used the ODUSSEAS software ([Antoniadis-Karnavas et al. 2020](#)), developed specifically for M-dwarfs, to measure the $[\text{Fe}/\text{H}]$ and $T_{\text{eff}\star}$ from the ESPRESSO spectra. Although ODUSSEAS was developed for spectra with resolutions from 48 000 to 115 000, it has been successfully used with ESPRESSO spec-

tra at their original 140 000 resolution ([Lillo-Box et al. 2020](#)). We obtained preliminary values of $[\text{Fe}/\text{H}] = -0.0024 \pm 0.104$, $T_{\text{eff}\star} = 3196 \pm 67 \text{ K}$, which were used as priors for the joint analysis³, in which a combination of the MIST evolution models, the transit-derived stellar bulk density, and the broad-band catalog photometry and parallax are employed to precisely constrain the host star parameters. To determine the spectral type, we used the PyHammer tool ([Roulston et al. 2020](#)) with the ESPRESSO spectra, which returned an M5 spectral type. However, colour index comparisons with the tables of [Pecaut & Mamajek \(2013\)](#) suggest an earlier spectral type of M3-M4, and visual inspection with the ‘eyecheck’ facility of PyHammer shows an M4 template is also a good match to the spectrum. Therefore, we adopt an M4 spectral type.

We modelled the observations both assuming a circular orbit for the planet, and allowing the orbit to have a non-zero eccentricity. We find that the free-eccentricity model produces an eccentricity consistent with zero ($e < 0.029$ at 95% confidence). A very low eccentricity is expected, given that we estimate a rapid tidal circularization timescale for this system of $\sim 6 \text{ Myr}$ ([Hut 1981](#)). We therefore adopt the parameters that result from assuming a circular orbit. Applying the transit least squares (TLS, [Hippke & Heller 2019](#)) algorithm to the HATSouth and *TESS* light curve residuals to the best-fit model finds no additional transit signals. The stellar parameters derived from the analysis assuming a circular orbit are listed in Table 4, while the planetary parameters are listed in Table 5. The best-fit model is shown in Figs. 1, 2, and 3. We note that the light curve uncertainties are scaled up in the fitting procedure to achieve a reduced χ^2 of unity, but the uncertainties shown in Fig. 2 have not been scaled.

The resulting $\sim 1\%$ and $\sim 0.5\%$ respective uncertainties on the derived stellar mass and radius are well below the respective $\sim 5\%$ and $\sim 4.2\%$ estimated systematic uncertainties of [Tayar et al. \(2022\)](#) for these parameters, which stem from inaccuracies in the fundamental observables and stellar evolution models. Likewise, the formal uncertainties of 7.4 K on the posterior stellar effective temperature and 0.017 dex on the metallicity are likely quite a bit smaller than the systematic uncertainties, which we may expect to be closer to the ODUSSEAS-derived uncertainties of $\sim 70 \text{ K}$ and $\sim 0.1 \text{ dex}$, respectively. However, as described in ([Eastman et al. 2022](#)),

³ An independent estimate of $T_{\text{eff}\star} = 3421 \pm 53 \text{ K}$ can be obtained using the absolute G magnitude M_G from Equation (11) of [Rabus et al. \(2019\)](#), which is consistent at $\approx 2\sigma$ with the value inferred from ODUSSEAS.

Table 1. Light curve data for TOI-3235.

BJD ^a	Mag ^b	σ_{Mag}	Mag(orig) ^c	Filter	Instrument
(2,450,000+)					
7853.13313	13.60729	0.03233	-0.02073	<i>r</i>	HATSouth/G701.3
7879.05934	13.62317	0.02532	-0.00485	<i>r</i>	HATSouth/G701.3
7801.28120	13.57721	0.03175	-0.05081	<i>r</i>	HATSouth/G701.3
7853.13745	13.66479	0.03355	0.03677	<i>r</i>	HATSouth/G701.3
7879.06378	13.65081	0.02521	0.02279	<i>r</i>	HATSouth/G701.3
7801.28524	13.61521	0.03411	-0.01281	<i>r</i>	HATSouth/G701.3
7801.29055	13.67750	0.05744	0.04948	<i>r</i>	HATSouth/G701.3
7853.14366	13.58338	0.03234	-0.04464	<i>r</i>	HATSouth/G701.3
7879.06997	13.59425	0.02449	-0.03377	<i>r</i>	HATSouth/G701.3
7853.14794	13.67704	0.03710	0.04902	<i>r</i>	HATSouth/G701.3

^a Barycentric Julian Date computed on the TDB system with correction for leap seconds.

^b The out-of-transit level has been subtracted. For observations made with the HATSouth instruments these magnitudes have been corrected for trends using the EPD and TFA procedures applied *prior* to fitting the transit model. This procedure may lead to an artificial dilution in the transit depths when used in its plain mode, instead of the signal reconstruction mode (Kovács et al. 2005). The blend factors for the HATSouth light curves are listed in Table 5. For observations made with follow-up instruments (anything other than “HATSouth” in the “Instrument” column), the magnitudes have been corrected for a quadratic trend in time, and for variations correlated with up to three PSF shape parameters, fit simultaneously with the transit.

^c Raw magnitude values without correction for the quadratic trend in time, or for trends correlated with the seeing.

NOTE— This table is available in a machine-readable form in the online journal. A portion is shown here for guidance regarding its form and content.

Table 2. Relative radial velocities and bisector spans from ESPRESSO for TOI-3235.

BJD	RV ^a	σ_{RV} ^b	BS	σ_{BS}	Phase
(2,450,000+)	(m s ⁻¹)	(m s ⁻¹)	(m s ⁻¹)	(m s ⁻¹)	
9612.80279	-185.54	4.18	0.224
9613.81343	126.16	3.91	0.613
9615.71703	-137.66	5.29	38.0	10.6	0.348
9617.71593	-121.86	4.26	32.6	8.5	0.119
9618.70340	0.95	5.52	-27.3	11.1	0.499
9619.86092	53.75	3.50	-12.7	7.0	0.946
9624.86523	129.76	4.23	-13.9	8.4	0.876

^a The zero-point of these velocities is arbitrary. An overall offset γ fitted to the velocities has been subtracted.

^b Internal errors excluding the component of astrophysical jitter considered in Section 3.

uncertainties smaller than the general error floors of Tayar et al. (2022) can be achieved for transiting plan-

ets by measuring the stellar density ρ_* directly from the transit and employing it in the derivation of other stellar parameters. Although our fit self-consistently accounts for the relation between the stellar density, transit parameters, M_* , L_* , R_* , and T_{eff} throughout the fit, as suggested by Eastman et al. (2022), and imposes a constraint that each link in the chain must match a stellar evolution model, it does not account for systematic errors in those models when imposing this constraint, and thus the formal uncertainties derived in this analysis are too small. Therefore, we conservatively adopt the error floors of Tayar et al. (2022), which we report in brackets in Table 4; for [Fe/H] we report the ODUSSEAS-derived uncertainty. These systematic uncertainties were formally propagated out to the planetary parameters. Regarding the planetary equilibrium temperature T_{eq} in particular, it is calculated under the assumptions of 0 albedo and full and instantaneous redistribution of heat, which are unlikely to hold completely in reality but provide a useful approximation.

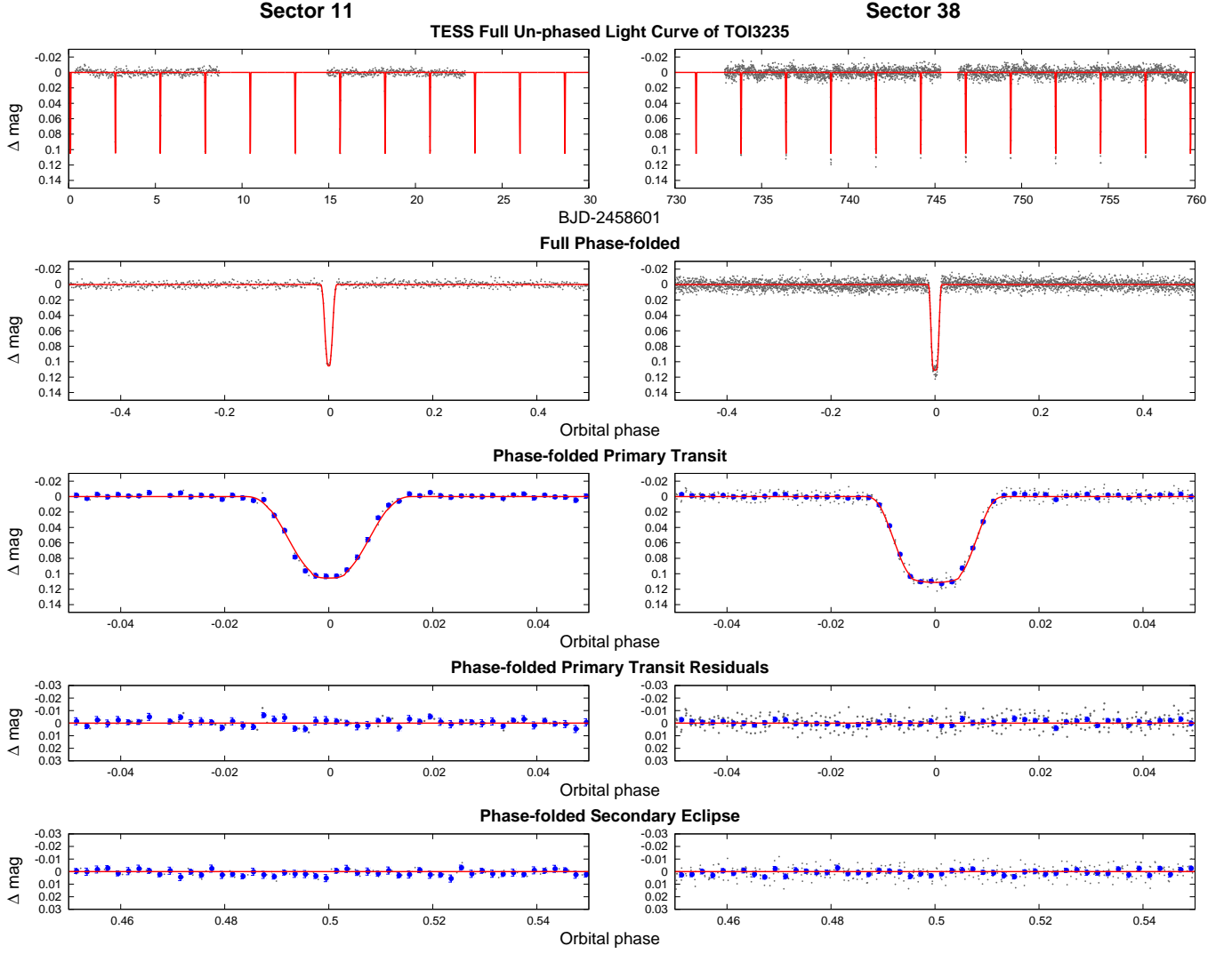


Figure 1. *TESS* long-cadence light curves for TOI-3235, for sector 11 (left, 30-minute cadence) and sector 38 (right, 10-minute cadence). For each sector, we show the full un-phased light curve as a function of time (*top*), the full phase-folded light curve (*second*), the phase-folded light curve zoomed-in on the planetary transit (*third*), the residuals from the best-fit model, phase-folded and zoomed-in on the planetary transit (*fourth*), and the phase-folded light curve zoomed-in on the secondary eclipse (*bottom*). The solid red line in each panel shows the model fit to the light curve. The blue filled circles show the light curve binned in phase with a bin size of 0.002. Other observations included in our analysis of this system are shown in Figures 2 and 3.

The formal fit gives a young age of $0.394^{+0.152}_{-0.090}$ Gyr for the host star. However, this is primarily driven by the photometry being somewhat blue compared to the model values (see Fig. 3, top right), which are known to be uncertain for M-dwarfs. We see no other evidence of youth such as flares. Likewise, the GLS periodogram of the HATSouth photometry shows a significant peak at 44.4264 ± 0.0010 days; taking this as the stellar rotation period, the relations of Engle & Guinan (2018) suggest a much larger age of ≈ 2.7 Gyr. We also used the BANYAN Σ tool (Gagné et al. 2018) to check the probability of TOI-3235 belonging to known young stel-

lar associations given its Gaia DR3 (Gaia Collaboration et al. 2022) proper motions and radial velocity, finding it has a 99.9% probability of being a field star.

Independent estimates of the stellar mass and radius can be obtained from the K_S magnitude using the mass-radius-luminosity relations of Mann et al. (2019) and Rabus et al. (2019). Applying these relations leads to a mass of $M_\star = 0.3605 \pm 0.087 M_\odot$ and a radius of $R_\star = 0.37 \pm 0.07 R_\odot$. While the radius is fully consistent with that obtained via global modelling, the mass is lower at 1.5σ . We choose to adopt the values from the global modelling, since it accounts for all

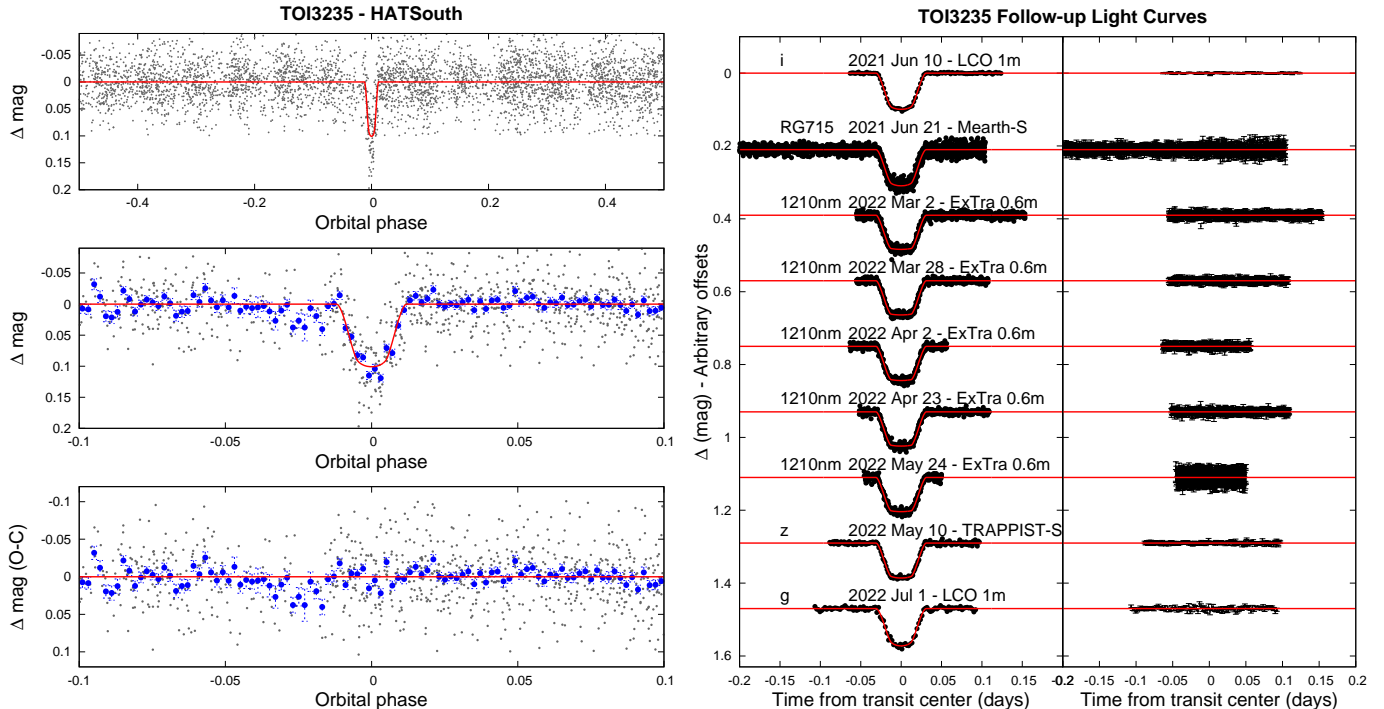


Figure 2. Ground-based photometry for the the transiting planet system TOI-3235. *Left:* Phase-folded unbinned full HATSouth light curve (top), light curve zoomed-in on the transit (middle), and residuals from the best-fit model zoomed-in on the transit (bottom). Solid red lines show the best-fit model. Blue circles show the light curves binned in phase with a bin size of 0.002. *Right:* Unbinned follow-up transit light curves corrected for instrumental trends fitted simultaneously with the transit model, which is overplotted (left), and residuals to the fit (right). Dates, filters and instruments are indicated. For ExTra we indicate the midpoint of the spectral range. The error bars represent the photon and background shot noise, plus the readout noise.

variables simultaneously. We also note that the planetary mass and radius calculated by employing the values obtained through the mass-radius-luminosity relations remain consistent with those computed from the global modelling values; thus, adopting the lower stellar mass from the mass-radius-luminosity relations would only make this giant planet even more unusual.

4. DISCUSSION AND CONCLUSIONS

TOI-3235 b is a close-in Jupiter with $M_p = 0.665 \pm 0.025 M_J$, $R_p = 1.017 \pm 0.044 R_J$, orbiting a $0.3939 \pm 0.0030 M_\odot$ M-dwarf with a period of $2.59261842 \pm 0.00000041$ days. To place it in the context of the M-dwarf planet population, in Figure 4 we plot TOI-3235 b together with all other well-characterized planets from the TEPICAT catalogue (Southworth 2011) hosted by stars with $M_\star \leq 0.61 M_\odot$ (limit chosen to include $M_\star \approx 0.6 M_\odot$ stars on K-M boundary). In mass-radius space (Fig. 4, top panel), TOI-3235 b joins a small cluster of ten giant planets with $0.8 R_J \leq R_p \leq 1.2 R_J$, and

$0.3 M_J \leq M_p \leq 1.5 M_J$. Most of these planets (HATS-6 b, Hartman et al. 2015; HATS-74 b and HATS-75 b, Jordán et al. 2022; Kepler-45 b, Johnson et al. 2012; TOI-530 b, Gan et al. 2022; TOI-3714 b, Cañas et al. 2022; WASP-80 b, Triaud et al. 2013) are hosted by early M-dwarfs with $M_\star \geq 0.5 M_\odot$. The sole other exception, aside from TOI-3235 b itself, is TOI-5205 b, a Jupiter-sized planet transiting a $0.392 M_\odot$ star (Kanodia et al. 2022). Save for TOI-530 b, which has a somewhat longer period of 6.39 d, these planets also cluster together in period-radius space (Fig. 4, centre panel), forming a group of mid-range close-in Jupiters with periods between 1.63 and 3.33 days. Likewise, all their host stars except WASP-80 are metal-rich (Fig. 4, bottom panel), in contrast to the wide range of metallicities shown by the host stars of the lower-mass planets. In particular, TOI-3235 has a metallicity of 0.26. These higher metallicities are consistent with previous findings (e.g. Johnson & Apps 2009; Rojas-Ayala et al. 2010) that M-dwarfs hosting giant planets tend to be metal-rich. The stellar mass vs planet mass diagram shown in this last panel also highlights the uniqueness of TOI-3235 b and its near twin TOI-5205 b, which inhabit an otherwise empty region of this parameter space.

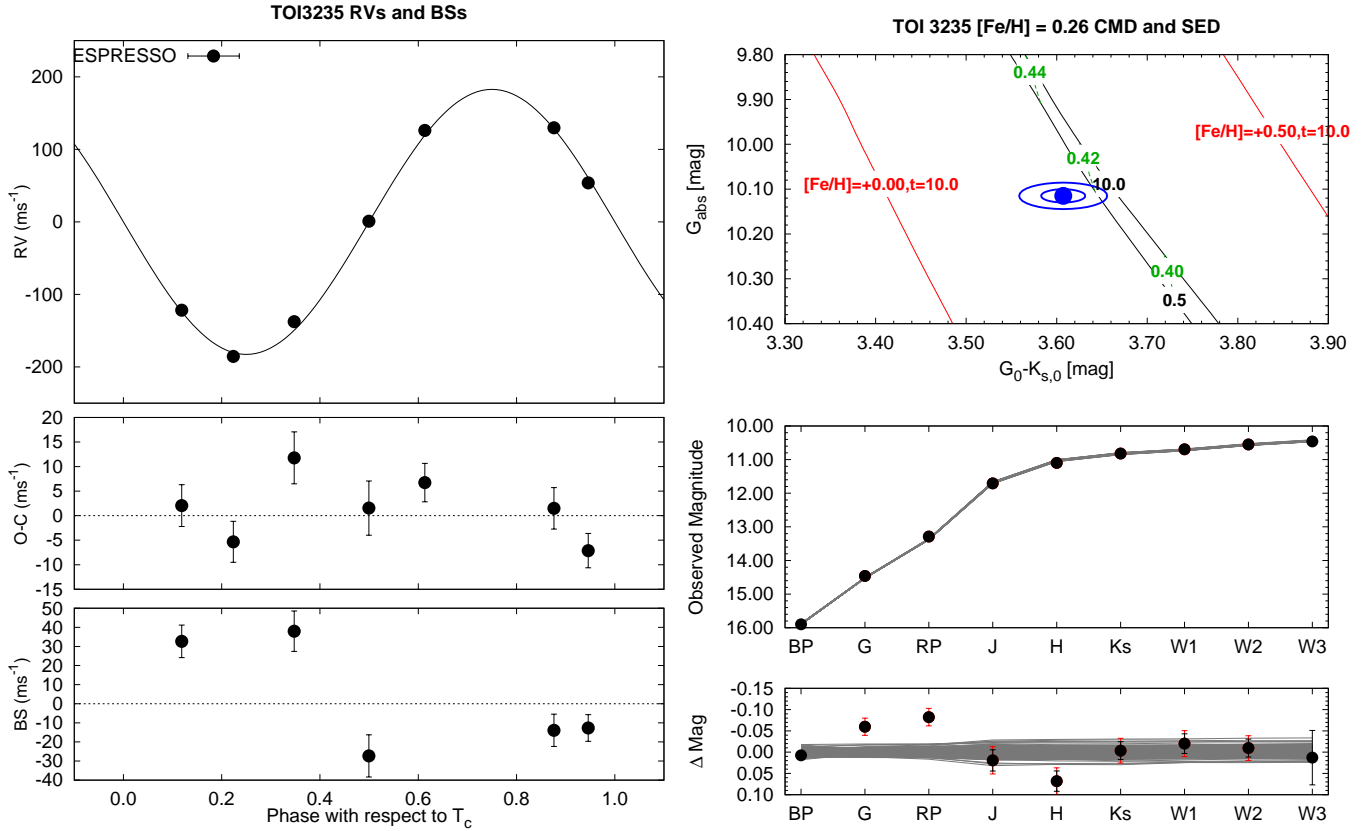


Figure 3. *Left:* High-precision RVs from ESPRESSO/VLT phased with respect to the mid-transit time, together with the best-fit model, where the center-of-mass velocity has been subtracted (top); RV $O-C$ residuals (centre); and bisector spans (bottom). Error bars include the estimated jitter, which is a free parameter in the fitting. *Top Right:* Absolute G magnitude vs. the de-reddened $G-K_S$ color from Gaia DR2 and 2MASS (filled blue circle) and 1σ and 2σ confidence regions, including estimated systematic errors in the photometry (blue lines), compared to theoretical isochrones (black lines, ages listed in Gyr) and stellar evolution tracks (green dashed lines, mass listed in solar masses) from the MIST models interpolated at the best-estimate value for the host metallicity. The red lines show isochrones at higher and lower metallicities than the best-estimate value, labelled with their metallicity and age in Gyr. *Bottom Right:* SED as measured via broadband photometry through the listed filters (top), and $O-C$ residuals from the best-fit model (bottom). We plot the observed magnitudes without correcting for distance or extinction. Overplotted are 200 model SEDs randomly selected from the MCMC posterior distribution produced through the global analysis (gray lines). Black error bars show the catalog errors for the broad-band photometry measurements; red error bars add an assumed 0.02 mag systematic uncertainty in quadrature to the catalog errors. These latter uncertainties are used in the fit.

Despite their clustering in mass-radius space, this group of giant planets spans a fairly wide range of densities, ranging from the very low-density HATS-6 b ($\rho \approx 0.4 \text{ g/cm}^3$) to the Jupiter-analogue TOI-5205 b ($\rho \approx 1.3 \text{ g/cm}^3$) and the high-density HATS-74 b ($\rho \approx 1.6 \text{ g/cm}^3$). TOI-3235 b sits in the centre of the range, with $\rho \approx 0.78 \text{ g/cm}^3$, comparable to the density of Saturn. They are all close to the peak of the theoretical mass-radius relationship derived by Mordasini et al. (2012) (Fig. 4, top panel, where we show the relationships for both the full synthetic population, and for planets with a $< 1 \text{ au}$); save for TOI-530 b, HATS-74 b, and HATS-75 b, which sit on the curve for planets with a $< 1 \text{ au}$, and TOI-5205 b, which is consistent with it within error bars, all have larger radii than

predicted. However, although all ten of these giants have periods shorter than the typical 10 d limit taken for hot Jupiters, they have equilibrium temperatures of $\approx 600 - 900 \text{ K}$ (Fig. 4, centre panel), well below the 1000 K limit at which the incident flux is expected to begin to inflate the radii (Miller & Fortney 2011; Demory & Seager 2011; Sarkis et al. 2021). It is also interesting to note that the low-mass planets generally have smaller radii than predicted, suggesting the theoretical relationship - derived from a synthetic population with a fixed stellar mass of $M_* = 1 M_\odot$ - may not be a good fit to M-dwarf planets overall.

The similarities between these giant planets may point to similar formation and migration histories. However, the differences in host star mass indicate caution; we

Table 3. Astrometric, Spectroscopic and Photometric parameters for TOI-3235

Parameter	Value	Source
Astrometric properties and cross-identifications		
2MASS-ID.....	2MASS 13495398-4603583	
TIC-ID.....	TIC 243641947	
Gaia DR3-ID.....	GAIA DR3 6107144260251920000	
R.A. (J2000).....	13 ^h 49 ^m 53.9777 ^s	Gaia DR3
Dec. (J2000).....	−46°03′58.4541″	Gaia DR3
$\mu_{R.A.}$ (mas yr ^{−1}).....	−170.503 ± 0.028	Gaia DR3
$\mu_{Dec.}$ (mas yr ^{−1}).....	−64.264 ± 0.023	Gaia DR3
parallax (mas).....	13.781 ± 0.027	Gaia DR3
radial velocity (km s ^{−1}).....	−14.96 ± 2.72	Gaia DR3
Spectroscopic properties		
$T_{\text{eff}\star}$ (K).....	3196 ± 67	ODUSSEAS/ESPRESSO ^a
[Fe/H].....	−0.02 ± 0.10	ODUSSEAS/ESPRESSO ^a
Spectral type.....	M4	this work
Photometric properties^b		
G (mag).....	14.4605 ± 0.0028	Gaia DR3
BP (mag).....	15.9000 ± 0.0042	Gaia DR3
RP (mag).....	13.2881 ± 0.0038	Gaia DR3
J (mag).....	11.706 ± 0.025	2MASS
H (mag).....	11.099 ± 0.024	2MASS
K_s (mag).....	10.819 ± 0.021	2MASS
$W1$ (mag).....	10.694 ± 0.023	WISE
$W2$ (mag).....	10.548 ± 0.021	WISE
$W3$ (mag).....	10.458 ± 0.064	WISE

^a The ODUSSEAS-derived $T_{\text{eff}\star}$ and [Fe/H] are not the final adopted parameters, but are used as priors for the global modelling.

^b The listed uncertainties for the photometry are taken from the catalogs. For the analysis we assume a systematic uncertainty floor of 0.02 mag.

Table 4. Derived stellar parameters for TOI-3235

Parameter	Value
M_\star (M_\odot).....	0.3939 ± 0.0030 (±0.020)
R_\star (R_\odot).....	0.3697 ± 0.0018 (±0.016)
$\log g_\star$ (cgs).....	4.8976 ± 0.0035 (±0.063)
ρ_\star (g cm ^{−3}).....	10.99 ± 0.13
L_\star (L_\odot).....	0.01623 ± 0.00018 (±0.00039)
$T_{\text{eff}\star}$ (K).....	3388.8 ± 5.9 (±68)
[Fe/H] (dex).....	0.264 ^{+0.013} _{−0.017} (±0.1)
A_V (mag).....	0.064 ± 0.021
Distance (pc).....	72.50 ± 0.12

NOTE— The listed parameters are those determined through the joint analysis described in Section 3 assuming a circular orbit for the planet. The first uncertainties listed for each parameter are the statistical uncertainties from the fit, not including systematic errors. Values in brackets report the estimated uncertainty floors due to inaccuracies in the fundamental observables and/or the MIST stellar evolution models, where appropriate. These latter floors were formally propagated to the planetary parameter uncertainties.

may be seeing two distinct populations, one corresponding to early M-dwarfs and one corresponding to later M-dwarfs. It is thus particularly interesting and relevant to compare TOI-3235 b to TOI-5205 b. Like TOI-5205,

TOI-3235 sits on the edge of the Jao Gap, a narrow gap in the Hertzsprung–Russell Diagram first identified by Jao et al. (2018) in Gaia data and linked by the authors to the transition between partially and fully convective stars, with $M_G = 10.04 \pm 0.95$ (Anders et al. 2022), and $B_P - R_P \approx 2.6$ (Gaia Collaboration et al. 2022). Both these stars are therefore in the transition region between partially and fully convective M-dwarfs, and as such are likely to undergo periodic changeovers from partially to fully convective and vice versa, that alter their radius and luminosity (e.g. van Saders & Pinsonneault 2012; Baraffe & Chabrier 2018). As noted by Kanodia et al. (2022), these oscillations may impact the planetary orbital parameters and equilibrium temperature. It is possible that the similar planets of these similar stars may share similar formation and/or evolution histories. Kanodia et al. (2022) studied the disk mass necessary to form TOI-5205 b. Since the host stars have the same mass, we can extrapolate from their analysis; the main difference is that TOI-3235 b is rather less massive than TOI-5205 b. As regards planetary heavy-element mass, using the relations of Thorngren et al. (2016) we find a heavy-element mass of $M_Z \sim 45M_\oplus$, corresponding to 75% of that of TOI-5205 b; therefore, assuming a solid core and scaling the results of Kanodia et al. (2022), the required disk mass for TOI-3235 b becomes $\sim 2\% - 23\%$ the mass of the host star for 100% – 10% formation effi-

Table 5. Adopted orbital and planetary parameters for TOI-3235 b

Parameter	Value
Light curve parameters	
P (days)	$2.59261842 \pm 0.00000041$
T_C (BJD-TDB) ^a	$2459690.001730 \pm 0.000045$
T_{14} (days) ^a	0.06165 ± 0.00021
$T_{12} = T_{34}$ (days) ^a	0.01765 ± 0.00030
a/R_*	15.75 ± 0.73
ζ/R_* ^b	44.41 ± 0.32
R_p/R_*	0.2828 ± 0.0016
b^2	$0.261^{+0.012}_{-0.012}$
$b \equiv a \cos i/R_*$	$0.511^{+0.011}_{-0.012}$
i (deg)	88.140 ± 0.046
Dilution factors ^c	
HAT G701/3	0.982 ± 0.022
HAT G701/4	0.957 ± 0.027
TESS Sector 11	1.084 ± 0.011
TESS Sector 38	1.1248 ± 0.0088
Limb-darkening coefficients ^d	
c_1, T	0.24 ± 0.12
c_2, T	0.33 ± 0.16
c_1, g	0.31 ± 0.12
c_2, g	0.35 ± 0.14
c_1, r	0.41 ± 0.15
c_2, r	0.32 ± 0.16
c_1, z	$0.140^{+0.106}_{-0.081}$
c_2, z	0.17 ± 0.13
$c_1, RG715$	0.30 ± 0.11
$c_2, RG715$	$0.26^{+0.11}_{-0.15}$
RV parameters	
K (m s^{-1})	182.9 ± 3.3
e ^e	< 0.029
RV jitter ESPRESSO (m s^{-1})	< 9.6
Planetary parameters	
M_p (M_J)	0.665 ± 0.025
R_p (R_J)	1.017 ± 0.044
$C(M_p, R_p)$ ^g	0.09
ρ_p (g cm^{-3})	0.78 ± 0.11
$\log g_p$ (cgs)	3.202 ± 0.041
a (AU)	0.02709 ± 0.00046
T_{eq} (K)	604 ± 19
Θ ^h	0.0896 ± 0.0042
$\log_{10}(F)$ (cgs) ⁱ	7.479 ± 0.018

NOTE— We adopt a model in which the orbit is assumed to be circular. See the discussion in Section 3.

^a Times are in Barycentric Julian Date calculated on the Barycentric Dynamical Time (TDB) system. T_C : Reference epoch of mid transit that minimizes the correlation with the orbital period. T_{14} : total transit duration, time between first to last contact; $T_{12} = T_{34}$: ingress/egress time, time between first and second, or third and fourth contact.

^b Reciprocal of the half duration of the transit used as a jump parameter in our MCMC analysis in place of a/R_* . It is related to a/R_* by the expression $\zeta/R_* = a/R_*(2\pi(1 + e \sin \omega))/(P\sqrt{1 - b^2}\sqrt{1 - e^2})$ (Bakos et al. 2010).

^c Scaling factor applied to the model transit fit to the HATSouth and TESS light curves. It accounts for dilution of the transit due to blending from neighboring stars, over-filtering of the light curve, or over-correction of dilution in the TESS SPOC light curves. These factors are varied in the fit, with independent values adopted for each light curve.

^d Values for a quadratic law. The limb-darkening parameters were directly varied in the fit, using the tabulations from Claret et al. (2012, 2013); Claret (2018) to place Gaussian priors on their values, assuming a prior uncertainty of 0.2 for each coefficient.

^e 95% confidence upper limit on the eccentricity determined when $\sqrt{e} \cos \omega$ and $\sqrt{e} \sin \omega$ are allowed to vary in the fit.

^f Term added in quadrature to the formal RV uncertainties for each instrument. It is a free parameter in the fitting routine.

^g Correlation coefficient between the planetary mass M_p and radius R_p estimated from the posterior parameter distribution.

^h The Safronov number is given by $\Theta = \frac{1}{2}(V_{\text{esc}}/V_{\text{orb}})^2 = (a/R_p)(M_p/M_*)$ (see Hansen & Barman 2007).

ⁱ Incoming flux per unit surface area, averaged over the orbit.

ciency respectively. While lower than the disk mass required to explain TOI-5205 b, given typical disk masses of the order of $\sim 0.1 - 5\%$ (Pascucci et al. 2016), the formation of TOI-3235 b still requires either an extremely high formation efficiency or a very massive disk.

TOI-3235 b also shows high potential for atmospheric characterization. We compute a Transmission Spectroscopy Metric (TSM, Kempton et al. 2018) of ≈ 160 , assuming a scale factor of 1.15. Comparing it to the group of M-dwarf planets it clusters with in mass-period-radius space, TOI-3235 b has the second-highest TSM, surpassed only by WASP-80 b (TSM ≈ 290), and notably higher than its analogue TOI-5205 b (TSM ≈ 100). Atmospheric characterization can help place constraints on the formation and migration history (e.g. Hobbs et al. 2022; Mollière et al. 2022) of this unexpected planet.

Facilities: TESS, HATSouth, MEarth-South, TRAPPIST-South, LCOGT, ExTrA, ESPRESSO, Gaia, Exoplanet Archive

Software: FITSH (Pál 2012), BLS (Kovács et al. 2002), VARTOOLS (Hartman & Bakos 2016), CERES (Brahm et al. 2017a), ZASPE (Brahm et al. 2017b), ODUSSEAS (Antoniadis-Karnavas et al. 2020), AstroImageJ (Collins et al. 2017), TAPIR (Jensen 2013b)

We thank the referee for their helpful comments that improved this paper.

This paper includes data collected by the TESS mission, which are publicly available from the Mikulski Archive for Space Telescopes (MAST). The specific observations analyzed can be accessed via [10.17909/mdsd-2297](https://archive.stsci.edu/mast/10.17909/mdsd-2297). Funding for the TESS mission is provided by NASA’s Science Mission directorate.

This research has made use of the Exoplanet Follow-up Observation Program website, which is operated by the California Institute of Technology, under contract with the National Aeronautics and Space Administration under the Exoplanet Exploration Program.

We acknowledge the use of public TESS data from pipelines at the TESS Science Office and at the TESS Science Processing Operations Center.

Resources supporting this work were provided by the NASA High-End Computing (HEC) Program through the NASA Advanced Supercomputing (NAS) Division at Ames Research Center for the production of the SPOC data products.

Based on observations collected at the European Organisation for Astronomical Research in the Southern Hemisphere under ESO programme 0108.C-0123(A).

A.J., R.B. and M.H. acknowledge support from ANID - Millennium Science Initiative - ICN12_009. A.J. acknowledges additional support from FONDECYT project 1210718. R.B. acknowledges support from FONDECYT Project 1120075 and from project IC120009 “Millennium Institute of Astrophysics (MAS)” of the Millennium Science Initiative. This work was funded by the Data Observatory Foundation.

The MEarth Team gratefully acknowledges funding from the David and Lucile Packard Fellowship for Science and Engineering (awarded to D.C.). This material is based upon work supported by the National Science Foundation under grants AST-0807690, AST-1109468, AST-1004488 (Alan T. Waterman Award), and AST-1616624, and upon work supported by the National Aeronautics and Space Administration under Grant No. 80NSSC18K0476 issued through the XRP Program. This work is made possible by a grant from the John Templeton Foundation. The opinions expressed in this publication are those of the authors and do not necessarily reflect the views of the John Templeton Foundation.

The research leading to these results has received funding from the ARC grant for Concerted Research Actions, financed by the Wallonia-Brussels Federation. TRAPPIST is funded by the Belgian Fund for Scientific Research (Fond National de la Recherche Scientifique, FNRS) under the grant PDR T.0120.21. MG is F.R.S.-FNRS Research Director and EJ is F.R.S.-FNRS Senior Research Associate. Observations were carried out from ESO La Silla Observatory.

The postdoctoral fellowship of KB is funded by F.R.S.-FNRS grant T.0109.20 and by the Francqui Foundation.

This work makes use of observations from the LCOGT network. Part of the LCOGT telescope time was granted by NOIRLab through the Mid-Scale Innovations Program (MSIP). MSIP is funded by NSF.

Based on data collected under the ExTrA project at the ESO La Silla Paranal Observatory. ExTrA is a project of Institut de Planétologie et d’Astrophysique de Grenoble (IPAG/CNRS/UGA), funded by the European Research Council under the ERC Grant Agreement n. 337591-ExTrA. This work has been supported by a grant from Labex OSUG@2020 (Investissements d’avenir – ANR10 LABX56). This work has been carried out within the framework of the NCCR PlanetS supported by the Swiss National Science Foundation. This work has been carried out within the framework of the National Centre of Competence in Research PlanetS supported by the Swiss National Science Foundation under grants 51NF40_182901 and 51NF40_205606. The authors acknowledge the financial support of the SNSF.

This publication benefits from the support of the French Community of Belgium in the context of the FRIA Doctoral Grant awarded to MT.

The contributions at the Mullard Space Science Laboratory by E.M.B. have been supported by STFC through the consolidated grant ST/W001136/1.

REFERENCES

- Almenara, J. M., Bonfils, X., Forveille, T., et al. 2022, arXiv e-prints, arXiv:2210.10909.
<https://arxiv.org/abs/2210.10909>
- Anders, F., Khalatyan, A., Queiroz, A. B. A., et al. 2022, *A&A*, 658, A91, doi: [10.1051/0004-6361/202142369](https://doi.org/10.1051/0004-6361/202142369)
- Antoniadis-Karnavas, A., Sousa, S. G., Delgado-Mena, E., et al. 2020, *A&A*, 636, A9, doi: [10.1051/0004-6361/201937194](https://doi.org/10.1051/0004-6361/201937194)
- Bakos, G. Á., Torres, G., Pál, A., et al. 2010, *ApJ*, 710, 1724, doi: [10.1088/0004-637X/710/2/1724](https://doi.org/10.1088/0004-637X/710/2/1724)
- Bakos, G. Á., Csubry, Z., Penev, K., et al. 2013, *PASP*, 125, 154, doi: [10.1086/669529](https://doi.org/10.1086/669529)
- Bakos, G. Á., Bayliss, D., Bento, J., et al. 2020, *AJ*, 159, 267, doi: [10.3847/1538-3881/ab8ad1](https://doi.org/10.3847/1538-3881/ab8ad1)
- Baraffe, I., & Chabrier, G. 2018, *A&A*, 619, A177, doi: [10.1051/0004-6361/201834062](https://doi.org/10.1051/0004-6361/201834062)
- Bayliss, D., Gillen, E., Eigmüller, P., et al. 2018, *MNRAS*, 475, 4467, doi: [10.1093/mnras/stx2778](https://doi.org/10.1093/mnras/stx2778)
- Bonfils, X., Almenara, J. M., Jocu, L., et al. 2015, in *Society of Photo-Optical Instrumentation Engineers (SPIE) Conference Series*, Vol. 9605, *Techniques and Instrumentation for Detection of Exoplanets VII*, ed. S. Shaklan, 96051L, doi: [10.1117/12.2186999](https://doi.org/10.1117/12.2186999)
- Boss, A. P. 2006, *ApJ*, 643, 501, doi: [10.1086/501522](https://doi.org/10.1086/501522)
- Bovy, J., Rix, H.-W., Green, G. M., Schlafly, E. F., & Finkbeiner, D. P. 2016, *ApJ*, 818, 130, doi: [10.3847/0004-637X/818/2/130](https://doi.org/10.3847/0004-637X/818/2/130)
- Brahm, R., Jordán, A., & Espinoza, N. 2017a, *Publications of the Astronomical Society of the Pacific*, 129, 034002, doi: [10.1088/1538-3873/aa5455](https://doi.org/10.1088/1538-3873/aa5455)
- Brahm, R., Jordán, A., Hartman, J., & Bakos, G. 2017b, *MNRAS*, 467, 971, doi: [10.1093/mnras/stx144](https://doi.org/10.1093/mnras/stx144)
- Brown, T. M., Baliber, N., Bianco, F. B., et al. 2013, *PASP*, 125, 1031, doi: [10.1086/673168](https://doi.org/10.1086/673168)

- Burn, R., Schlecker, M., Mordasini, C., et al. 2021, arXiv e-prints, arXiv:2105.04596.
<https://arxiv.org/abs/2105.04596>
- Cañas, C. I., Kanodia, S., Bender, C. F., et al. 2022, *AJ*, 164, 50, doi: [10.3847/1538-3881/ac7804](https://doi.org/10.3847/1538-3881/ac7804)
- Caldwell, D. A., Tenenbaum, P., Twicken, J. D., et al. 2020, *Research Notes of the American Astronomical Society*, 4, 201, doi: [10.3847/2515-5172/abc9b3](https://doi.org/10.3847/2515-5172/abc9b3)
- Chabrier, G., & Baraffe, I. 1997, *A&A*, 327, 1039.
<https://arxiv.org/abs/astro-ph/9704118>
- Choi, J., Dotter, A., Conroy, C., et al. 2016, *ApJ*, 823, 102, doi: [10.3847/0004-637X/823/2/102](https://doi.org/10.3847/0004-637X/823/2/102)
- Claret, A. 2018, *A&A*, 618, A20, doi: [10.1051/0004-6361/201833060](https://doi.org/10.1051/0004-6361/201833060)
- Claret, A., Hauschildt, P. H., & Witte, S. 2012, *A&A*, 546, A14, doi: [10.1051/0004-6361/201219849](https://doi.org/10.1051/0004-6361/201219849)
- . 2013, *A&A*, 552, A16, doi: [10.1051/0004-6361/201220942](https://doi.org/10.1051/0004-6361/201220942)
- Collins, K. A., Kielkopf, J. F., Stassun, K. G., & Hessman, F. V. 2017, *AJ*, 153, 77, doi: [10.3847/1538-3881/153/2/77](https://doi.org/10.3847/1538-3881/153/2/77)
- Demory, B.-O., & Seager, S. 2011, *ApJS*, 197, 12, doi: [10.1088/0067-0049/197/1/12](https://doi.org/10.1088/0067-0049/197/1/12)
- Dotter, A. 2016, *ApJS*, 222, 8, doi: [10.3847/0067-0049/222/1/8](https://doi.org/10.3847/0067-0049/222/1/8)
- Dressing, C. D., & Charbonneau, D. 2015, *ApJ*, 807, 45, doi: [10.1088/0004-637X/807/1/45](https://doi.org/10.1088/0004-637X/807/1/45)
- Eastman, J. D., Diamond-Lowe, H., & Tayar, J. 2022, arXiv e-prints, arXiv:2209.14301.
<https://arxiv.org/abs/2209.14301>
- Engle, S. G., & Guinan, E. F. 2018, *Research Notes of the American Astronomical Society*, 2, 34, doi: [10.3847/2515-5172/aab1f8](https://doi.org/10.3847/2515-5172/aab1f8)
- Fausnaugh, M. M., Burke, C. J., Ricker, G. R., & Vanderspek, R. 2020, *Research Notes of the American Astronomical Society*, 4, 251, doi: [10.3847/2515-5172/abd63a](https://doi.org/10.3847/2515-5172/abd63a)
- Freudling, W., Romaniello, M., Bramich, D. M., et al. 2013, *A&A*, 559, A96, doi: [10.1051/0004-6361/201322494](https://doi.org/10.1051/0004-6361/201322494)
- Gagné, J., Mamajek, E. E., Malo, L., et al. 2018, *ApJ*, 856, 23, doi: [10.3847/1538-4357/aaae09](https://doi.org/10.3847/1538-4357/aaae09)
- Gaia Collaboration, Brown, A. G. A., Vallenari, A., et al. 2018, *A&A*, 616, A1, doi: [10.1051/0004-6361/201833051](https://doi.org/10.1051/0004-6361/201833051)
- Gaia Collaboration, Vallenari, A., Brown, A. G. A., et al. 2022, arXiv e-prints, arXiv:2208.00211, doi: [10.48550/arXiv.2208.00211](https://doi.org/10.48550/arXiv.2208.00211)
- Gan, T., Lin, Z., Wang, S. X., et al. 2022, *MNRAS*, 511, 83, doi: [10.1093/mnras/stab3708](https://doi.org/10.1093/mnras/stab3708)
- Garcia, L. J., Timmermans, M., Pozuelos, F. J., et al. 2021, *MNRAS*, doi: [10.1093/mnras/stab3113](https://doi.org/10.1093/mnras/stab3113)
- Gillon, M., Jehin, E., Magain, P., et al. 2011, *EPJ Web of Conferences*, 11, 06002, doi: [10.1051/epjconf/20101106002](https://doi.org/10.1051/epjconf/20101106002)
- Guerrero, N. M., Seager, S., Huang, C. X., et al. 2021, *ApJS*, 254, 39, doi: [10.3847/1538-4365/abefel](https://doi.org/10.3847/1538-4365/abefel)
- Hansen, B. M. S., & Barman, T. 2007, *ApJ*, 671, 861, doi: [10.1086/523038](https://doi.org/10.1086/523038)
- Hartman, J. D., & Bakos, G. Á. 2016, *Astronomy and Computing*, 17, 1, doi: [10.1016/j.ascom.2016.05.006](https://doi.org/10.1016/j.ascom.2016.05.006)
- Hartman, J. D., Bayliss, D., Brahm, R., et al. 2015, *AJ*, 149, 166, doi: [10.1088/0004-6256/149/5/166](https://doi.org/10.1088/0004-6256/149/5/166)
- Hartman, J. D., Bakos, G. Á., Bayliss, D., et al. 2019, *AJ*, 157, 55, doi: [10.3847/1538-3881/aaf8b6](https://doi.org/10.3847/1538-3881/aaf8b6)
- Hippke, M., & Heller, R. 2019, *A&A*, 623, A39, doi: [10.1051/0004-6361/201834672](https://doi.org/10.1051/0004-6361/201834672)
- Hirano, T., Dai, F., Gandolfi, D., et al. 2018, *AJ*, 155, 127, doi: [10.3847/1538-3881/aaa9c1](https://doi.org/10.3847/1538-3881/aaa9c1)
- Hobbs, R., Shorttle, O., & Madhusudhan, N. 2022, *MNRAS*, 516, 1032, doi: [10.1093/mnras/stac2106](https://doi.org/10.1093/mnras/stac2106)
- Hsu, D. C., Ford, E. B., & Terrien, R. 2020, *MNRAS*, 498, 2249, doi: [10.1093/mnras/staa2391](https://doi.org/10.1093/mnras/staa2391)
- Huang, C. X., Vanderburg, A., Pál, A., et al. 2020a, *Research Notes of the American Astronomical Society*, 4, 204, doi: [10.3847/2515-5172/abca2e](https://doi.org/10.3847/2515-5172/abca2e)
- . 2020b, *Research Notes of the American Astronomical Society*, 4, 206, doi: [10.3847/2515-5172/abca2d](https://doi.org/10.3847/2515-5172/abca2d)
- Hut, P. 1981, *A&A*, 99, 126
- Irwin, J. M., Berta-Thompson, Z. K., Charbonneau, D., et al. 2015, in *Cambridge Workshop on Cool Stars, Stellar Systems, and the Sun*, Vol. 18, 18th Cambridge Workshop on Cool Stars, Stellar Systems, and the Sun, 767–772. <https://arxiv.org/abs/1409.0891>
- Jao, W.-C., Henry, T. J., Gies, D. R., & Hambly, N. C. 2018, *ApJL*, 861, L11, doi: [10.3847/2041-8213/aacdf6](https://doi.org/10.3847/2041-8213/aacdf6)
- Jehin, E., Gillon, M., Queloz, D., et al. 2011, *The Messenger*, 145, 2
- Jenkins, J. M., Twicken, J. D., McCauliff, S., et al. 2016, in *Proc. SPIE*, Vol. 9913, *Software and Cyberinfrastructure for Astronomy IV*, 99133E, doi: [10.1117/12.2233418](https://doi.org/10.1117/12.2233418)
- Jensen, E. 2013a, Tapir: A web interface for transit/eclipse observability, *Astrophysics Source Code Library*, record ascl:1306.007. <http://ascl.net/1306.007>
- . 2013b, Tapir: A web interface for transit/eclipse observability, *Astrophysics Source Code Library*. <http://ascl.net/1306.007>
- Johnson, J. A., & Apps, K. 2009, *ApJ*, 699, 933, doi: [10.1088/0004-637X/699/2/933](https://doi.org/10.1088/0004-637X/699/2/933)
- Johnson, J. A., Gazak, J. Z., Apps, K., et al. 2012, *AJ*, 143, 111, doi: [10.1088/0004-6256/143/5/111](https://doi.org/10.1088/0004-6256/143/5/111)

- Jordán, A., Hartman, J. D., Bayliss, D., et al. 2022, *AJ*, 163, 125, doi: [10.3847/1538-3881/ac4a77](https://doi.org/10.3847/1538-3881/ac4a77)
- Kanodia, S., Mahadevan, S., Libby-Roberts, J., et al. 2022, arXiv e-prints, arXiv:2209.11160. <https://arxiv.org/abs/2209.11160>
- Kempton, E. M. R., Bean, J. L., Louie, D. R., et al. 2018, *PASP*, 130, 114401, doi: [10.1088/1538-3873/aadf6f](https://doi.org/10.1088/1538-3873/aadf6f)
- Kovács, G., Bakos, G., & Noyes, R. W. 2005, *MNRAS*, 356, 557, doi: [10.1111/j.1365-2966.2004.08479.x](https://doi.org/10.1111/j.1365-2966.2004.08479.x)
- Kovács, G., Zucker, S., & Mazeh, T. 2002, *A&A*, 391, 369, doi: [10.1051/0004-6361:20020802](https://doi.org/10.1051/0004-6361:20020802)
- Laughlin, G., Bodenheimer, P., & Adams, F. C. 2004, *ApJL*, 612, L73, doi: [10.1086/424384](https://doi.org/10.1086/424384)
- Lillo-Box, J., Figueira, P., Leleu, A., et al. 2020, *A&A*, 642, A121, doi: [10.1051/0004-6361/202038922](https://doi.org/10.1051/0004-6361/202038922)
- Mandel, K., & Agol, E. 2002, *ApJL*, 580, L171, doi: [10.1086/345520](https://doi.org/10.1086/345520)
- Mann, A. W., Dupuy, T., Kraus, A. L., et al. 2019, *ApJ*, 871, 63, doi: [10.3847/1538-4357/aaf3bc](https://doi.org/10.3847/1538-4357/aaf3bc)
- McCully, C., Volgenau, N. H., Harbeck, D.-R., et al. 2018, in *Society of Photo-Optical Instrumentation Engineers (SPIE) Conference Series*, Vol. 10707, Proc. SPIE, 107070K, doi: [10.1117/12.2314340](https://doi.org/10.1117/12.2314340)
- Miller, N., & Fortney, J. J. 2011, *ApJL*, 736, L29, doi: [10.1088/2041-8205/736/2/L29](https://doi.org/10.1088/2041-8205/736/2/L29)
- Modigliani, A., Freudling, W., Anderson, R. I., et al. 2020, in *Astronomical Society of the Pacific Conference Series*, Vol. 527, *Astronomical Data Analysis Software and Systems XXIX*, ed. R. Pizzo, E. R. Deul, J. D. Mol, J. de Plaa, & H. Verkouter, 667
- Mollière, P., Molyarova, T., Bitsch, B., et al. 2022, *ApJ*, 934, 74, doi: [10.3847/1538-4357/ac6a56](https://doi.org/10.3847/1538-4357/ac6a56)
- Morales, J. C., Mustill, A. J., Ribas, I., et al. 2019, *Science*, 365, 1441, doi: [10.1126/science.aax3198](https://doi.org/10.1126/science.aax3198)
- Mordasini, C., Alibert, Y., Georgy, C., et al. 2012, *A&A*, 547, A112, doi: [10.1051/0004-6361/201118464](https://doi.org/10.1051/0004-6361/201118464)
- Mulders, G. D. 2018, *Planet Populations as a Function of Stellar Properties*, ed. H. J. Deeg & J. A. Belmonte, 153, doi: [10.1007/978-3-319-55333-7_153](https://doi.org/10.1007/978-3-319-55333-7_153)
- Nutzman, P., & Charbonneau, D. 2008, *PASP*, 120, 317, doi: [10.1086/533420](https://doi.org/10.1086/533420)
- Pál, A. 2012, *MNRAS*, 421, 1825, doi: [10.1111/j.1365-2966.2011.19813.x](https://doi.org/10.1111/j.1365-2966.2011.19813.x)
- Pascucci, I., Testi, L., Herczeg, G. J., et al. 2016, *ApJ*, 831, 125, doi: [10.3847/0004-637X/831/2/125](https://doi.org/10.3847/0004-637X/831/2/125)
- Paxton, B., Bildsten, L., Dotter, A., et al. 2011, *ApJS*, 192, 3, doi: [10.1088/0067-0049/192/1/3](https://doi.org/10.1088/0067-0049/192/1/3)
- Paxton, B., Cantiello, M., Arras, P., et al. 2013, *ApJS*, 208, 4, doi: [10.1088/0067-0049/208/1/4](https://doi.org/10.1088/0067-0049/208/1/4)
- Paxton, B., Marchant, P., Schwab, J., et al. 2015, *ApJS*, 220, 15, doi: [10.1088/0067-0049/220/1/15](https://doi.org/10.1088/0067-0049/220/1/15)
- Pecaut, M. J., & Mamajek, E. E. 2013, *ApJS*, 208, 9, doi: [10.1088/0067-0049/208/1/9](https://doi.org/10.1088/0067-0049/208/1/9)
- Penev, K., Bakos, G. Á., Bayliss, D., et al. 2013, *AJ*, 145, 5, doi: [10.1088/0004-6256/145/1/5](https://doi.org/10.1088/0004-6256/145/1/5)
- Pepe, F., Cristiani, S., Rebolo, R., et al. 2021, *A&A*, 645, A96, doi: [10.1051/0004-6361/202038306](https://doi.org/10.1051/0004-6361/202038306)
- Rabus, M., Lachaume, R., Jordán, A., et al. 2019, *MNRAS*, 484, 2674, doi: [10.1093/mnras/sty3430](https://doi.org/10.1093/mnras/sty3430)
- Ricker, G. R., Winn, J. N., Vanderspek, R., et al. 2015, *Journal of Astronomical Telescopes, Instruments, and Systems*, 1, 014003, doi: [10.1117/1.JATIS.1.1.014003](https://doi.org/10.1117/1.JATIS.1.1.014003)
- Rojas-Ayala, B., Covey, K. R., Muirhead, P. S., & Lloyd, J. P. 2010, *ApJL*, 720, L113, doi: [10.1088/2041-8205/720/1/L113](https://doi.org/10.1088/2041-8205/720/1/L113)
- Roulston, B. R., Green, P. J., & Kesseli, A. Y. 2020, *ApJS*, 249, 34, doi: [10.3847/1538-4365/abale7](https://doi.org/10.3847/1538-4365/abale7)
- Sarkis, P., Mordasini, C., Henning, T., Marleau, G. D., & Mollière, P. 2021, *A&A*, 645, A79, doi: [10.1051/0004-6361/202038361](https://doi.org/10.1051/0004-6361/202038361)
- Schlecker, M., Burn, R., Sabotta, S., et al. 2022, *A&A*, 664, A180, doi: [10.1051/0004-6361/202142543](https://doi.org/10.1051/0004-6361/202142543)
- Skrutskie, M. F., Cutri, R. M., Stiening, R., et al. 2006, *AJ*, 131, 1163, doi: [10.1086/498708](https://doi.org/10.1086/498708)
- Smith, J. C., Stumpe, M. C., Van Cleve, J. E., et al. 2012, *PASP*, 124, 1000, doi: [10.1086/667697](https://doi.org/10.1086/667697)
- Sosnowska, D., Lovis, C., Figueira, P., et al. 2015, in *Astronomical Society of the Pacific Conference Series*, Vol. 495, *Astronomical Data Analysis Software and Systems XXIV (ADASS XXIV)*, ed. A. R. Taylor & E. Rosolowsky, 285. <https://arxiv.org/abs/1509.05584>
- Southworth, J. 2011, *MNRAS*, 417, 2166, doi: [10.1111/j.1365-2966.2011.19399.x](https://doi.org/10.1111/j.1365-2966.2011.19399.x)
- Stumpe, M. C., Smith, J. C., Catanzarite, J. H., et al. 2014, *PASP*, 126, 100, doi: [10.1086/674989](https://doi.org/10.1086/674989)
- Stumpe, M. C., Smith, J. C., Van Cleve, J. E., et al. 2012, *PASP*, 124, 985, doi: [10.1086/667698](https://doi.org/10.1086/667698)
- Tayar, J., Claytor, Z. R., Huber, D., & van Saders, J. 2022, *ApJ*, 927, 31, doi: [10.3847/1538-4357/ac4bbc](https://doi.org/10.3847/1538-4357/ac4bbc)
- Thorngren, D. P., Fortney, J. J., Murray-Clay, R. A., & Lopez, E. D. 2016, *ApJ*, 831, 64, doi: [10.3847/0004-637X/831/1/64](https://doi.org/10.3847/0004-637X/831/1/64)
- Triaud, A. H. M. J., Anderson, D. R., Collier Cameron, A., et al. 2013, *A&A*, 551, A80, doi: [10.1051/0004-6361/201220900](https://doi.org/10.1051/0004-6361/201220900)
- Twicken, J. D., Catanzarite, J. H., Clarke, B. D., and Girouard, F., et al. 2018, *PASP*, 130, 064502, doi: [10.1088/1538-3873/aab694](https://doi.org/10.1088/1538-3873/aab694)

van Saders, J. L., & Pinsonneault, M. H. 2012, *ApJ*, 751,
98, doi: [10.1088/0004-637X/751/2/98](https://doi.org/10.1088/0004-637X/751/2/98)

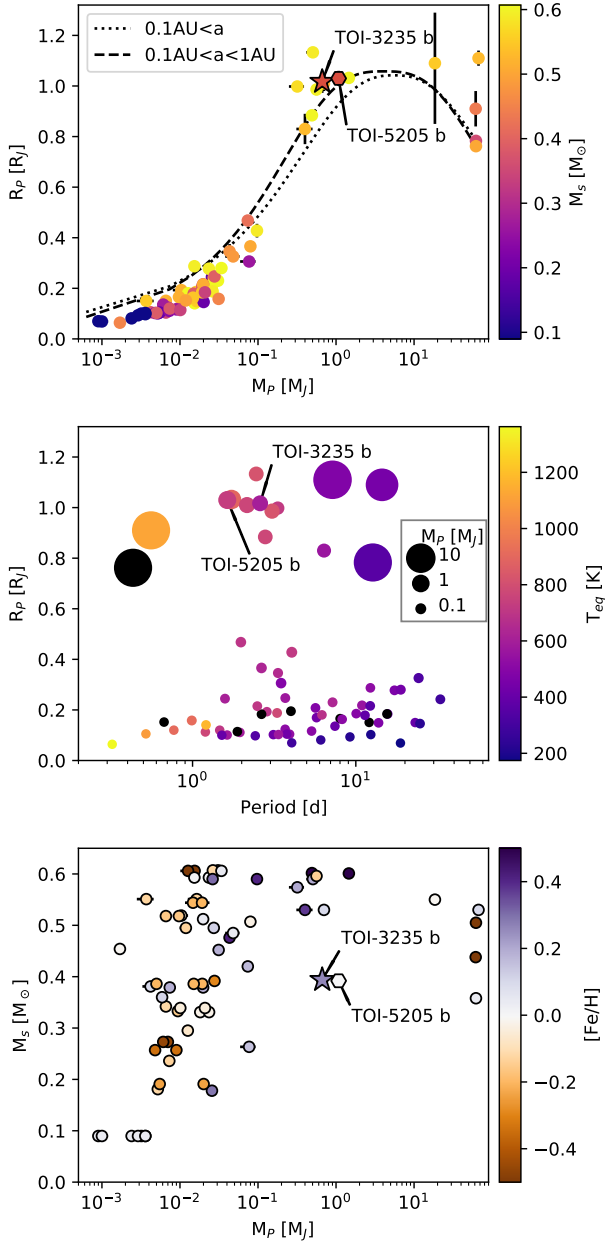


Figure 4. *Top:* Mass-radius diagram for M-dwarf planets with masses and radii measured to better than 25%, as reported in TEPCAT. The markers are colour-coded by host star mass. TOI-3235 b and its analogue TOI-5205 b are plotted with star and hexagon symbols respectively and labelled. Theoretical mass-radius curves from [Mordasini et al. \(2012\)](#) are plotted with dashed and dotted lines. *Centre:* Period-radius diagram for the same planets. The markers are scaled by planet mass and colour-coded by equilibrium temperature (black when it could not be computed). TOI-3235 b and TOI-5205 b are labelled. *Bottom:* Planet mass vs. stellar mass diagram for the same planets. The markers are colour-coded by host star metallicity. TOI-3235 b and TOI-5205 b are plotted with star and hexagon symbols respectively and labelled.